Research | Received 5 November 2024; Accepted Day Mon 2025; Published Day Mon 2025
https://doi.org/10.55092/neuroelectronics20250001

Advancing EEG classification for neurodegenerative conditions using BCI: a graph attention approach with phase synchrony

Rishan Patel[1,*], Ziyue Zhu[2], Barney Bryson[3], Tom Carlson[2], Dai Jiang[1] and Andreas Demosthenous[1,*]

[1] Electronic and Electrical Engineering, University College London, London, United Kingdom
[2] Aspire Create, University College London, London, United Kingdom
[3] Institute of Neurology, University College London, London, United Kingdom

* Correspondence authors; E-mails: uceerjp@ucl.ac.uk (R.P.); a.demosthenous@ucl.ac.uk (A.D.).

Abstract: Accurately classifying electroencephalogram (EEG) signals, especially for individuals with neurodegenerative conditions such as amyotrophic lateral sclerosis (ALS), poses a significant challenge due to high inter-subject and inter-session changes in signal. This study introduces a novel three-layer graph attention network (GAT) model for motor imagery (MI) classification, utilizing phase locking value (PLV) as the graph input. The GAT model outperforms state-of-the-art deep learning methods, demonstrating notable improvements with a two-class accuracy of 74.06% on an ALS dataset (approximately 320 trials collected over 1-2 months), and 71.89% on the BCI Comp IV 2a Dataset. This improvement demonstrates the effectiveness of graph-based representations to enhance classification performance for neurodegenerative conditions. There are statistically significant reductions in variance compared to state-of-the-art, due to subject-specific attention given by the model during testing. These results support the hypothesis that phase-locking value-based graph representations can enhance neural representations in BCIs, offering promising avenues for more personalized approaches in MI classification. This study highlights the potential for further optimizing GAT architectures and feature sets, pointing to future research directions that could improve performance and efficiency in MI classification tasks whilst establishing a lightweight methodology.

Keywords: motor imagery, amyotrophic lateral sclerosis, graph attention networks, electroencephalography, brain computer interface (BCI)

1. Introduction

Electroencephalography (EEG) measures electrical brain potentials through the scalp, reflecting the synaptic activity of large brain areas. It offers high temporal resolution to capture rapid changes in brain dynamics, which BCIs can utilize to decode neuronal information for controlling computers and devices. Users (including patients with motor impairments) can learn to modulate specific frequency bands recognized as sensorimotor rhythms (SMR), which are associated with imagined or executed movement originating around the sensorimotor cortex [1].

Motor impairments such as amyotrophic lateral sclerosis (ALS) cause the gradual degeneration of motor neurones, rendering functional control of muscles much more difficult as the disease progresses. This degeneration leads to significant changes in the patient's brains. ALS progression leads to cortical reconfiguration and degraded SMR control signals [2], often resulting in weaker or absent event-related desynchronisation (ERD), which is the decrease in relative power of a frequency band during motor execution and imagery. BCIs could improve patient quality of life through assistive technologies, supporting rehabilitation and replacing lost functionalities [3]. However, comprehensive end-user studies are lacking [3] where in clinical settings, BCI systems face challenges due to the non-stationarity of EEG signals as the disease progresses. Unfortunately, longitudinal experiments are scarce in addressing these issues [3].

Many studies highlight BCI inability (sometimes termed "BCI illiteracy"), where a minority of individuals (<50%) cannot achieve 70% accuracy using current systems and training protocols [4]. Studies have observed varying failure rates among participants in meeting specific thresholds: 48.7% of 99 participants [5], 37.5% of 80 participants [6], 45% of 40 participants [7], and 40.4% of 151 participants [8] did not meet the required 70%. Non-stationarity in EEG signals is a critical issue for BCI users, necessitating frequent model retraining due to various factors: covariate shifts (*e.g.*, environmental changes, electrode placement differences) affecting reliability, and user-specific variations (*e.g.*, brain anatomy, electrode-skin impedance, cognitive states) complicating model generalization across diverse populations. Addressing these challenges could significantly improve BCI utility in clinical settings by reducing the need for frequent recalibration thus enhancing long-term performance. These findings demonstrate the necessity for novel strategies to improve user performance and accessibility in BCI systems. Employing an approach that utilizes connectivity measures to identify unique spatio-temporal patterns could significantly enhance the analysis and classification of patient EEG data by means of personalisation.

Functional connectivity measures are becoming increasingly popular in EEG research, offering new insights into task-specific features and enabling advanced deep learning methodologies to capture complex spatial patterns. Daly et al [9] utilized phase synchronization through phase locking value (PLV) and empirical mode decomposition phase locking (EMDPL) to decode the imagined action of finger tapping, typically called motor imagery (MI) irrespective of motor task in 22 volunteers, achieving classification rates of at least 84% [9]. Reference [10] investigated the impact of phase synchrony on patients with neuromuscular disease (NMD) and its effect on MI. They compared NMD patients with controls to explore personalization in MI decoding. Their findings indicated that phase synchrony is a reliable feature for MI decoding in NMD, with rapid reorganization allowing timely MI decoding. Notably, NMD patients showed an inherent advantage in using phase synchrony for subject-specific models [10].

PLV representation of EEG can be remodeled as a network-level graph. This allows the introduction of graph-based models which have gained traction in various machine learning domains due to their ability to capture complex relationships within data. Graph neural networks (GNNs) have emerged as a unique solution to classifying graph and node level tasks in recent years, with successful applications in two main forms: Spectral and Spatial GNNs. Spatial GNNs take advantage of spatial features like the adjacency matrix, where nodes possess features which are aggregated in message passing [11]. In a limited survey on the classification of EEG signals using GNNs [11], it was found that the majority of studies focused on emotion classification, with MI classification being the third most common application, represented in fewer than ten papers [11]. This survey revealed that a substantial proportion of the

studies employed basic spatial graph convolutional networks (GCN). This trend may be attributed to the relative novelty of the field, resulting in limited experimentation with more sophisticated architectures. Additionally, there is a notable lack of generalization to external datasets and insufficient utilization of frequency band information in more complex ways. The authors in [11] recommend comparing more advanced GCN layers, such as graph attention networks (GATs), to enhance the generalizability of models. They also suggest integrating measures like cross-frequency coupling to better leverage frequency band information. An interesting study by Almohammadi et al [12] begins to build on these ideas where a filter banked PLV-Convolutional Neural Network (CNN) in a 4-class task for BCI Competition IV 2a was used. It takes advantage of the graphical structure of the data, whilst presenting as an image to a CNN, which demonstrates peak performance in the 4–8Hz filter bank [12].

GATs, a variant of graph convolutional networks (GCNs) designed for spatial feature representation, have demonstrated considerable potential in complex feature extraction tasks [13]. However, existing implementations often do not fully leverage connectivity measures, such as PLV. [14] demonstrates GATs on error related potentials (ErrPs) and Rapid Serial Visual Presentation, demonstrating impressive accuracies of 76% and 96% respectively. This methodology is inspired by EEGNet [14], but at the time of writing, there are still very few GAT representations of MI EEG in the literature. The spatio-temporal blend of PLV and deeper frequency information representation with GAT in MI remains an unexplored avenue which bears the burden of investigation considering there may be performance benefits for patients [10] as evidenced by [12, 14].

This paper introduces a novel model that leverages the spatially-distributed phase synchrony patterns with GATs for capturing dynamic relationships in MI EEG data. The methodology moves towards a solution for the lack of adequate control caused by BCI inefficiency, especially in end users such as ALS patients who have severely non-stationary EEG signals, which vary not only patient to patient, but session to session. The approach is tested on the benchmark BCI competition IV 2a dataset [15], demonstrating its performance against eight state-of-the-art models. The GAT is evaluated using a unique ALS dataset [16] collected over 1–2 months, showcasing its performance on intersubject and intersession variability, contributing to the development of models for end users and providing stronger evidence that patients with motor neural disease (MND), specifically ALS, benefit from specific methodologies for their unique disease. This is the first paper to test the efficacy of representing EEG as a graph in ALS patients along with the application of graph classification with an attention mechanism to classify MI over multiple sessions. The overarching goal is to develop methods that contribute to improving the quality of life of ALS patients using BCI, a task that is especially difficult due to the nature of this disease.

The remainder of this paper is organized as follows: Section 2 outlines the methodology, detailing the stages from PLV calculation to graph generation and the architecture of the GAT. Section 3 presents the experimental results and discusses the implications of the findings, focusing on enhanced accuracies for ALS compared to other models, inter-subject differences, and performance comparisons across cohorts. Section 4 concludes the paper and suggests future research directions.

2. Methods

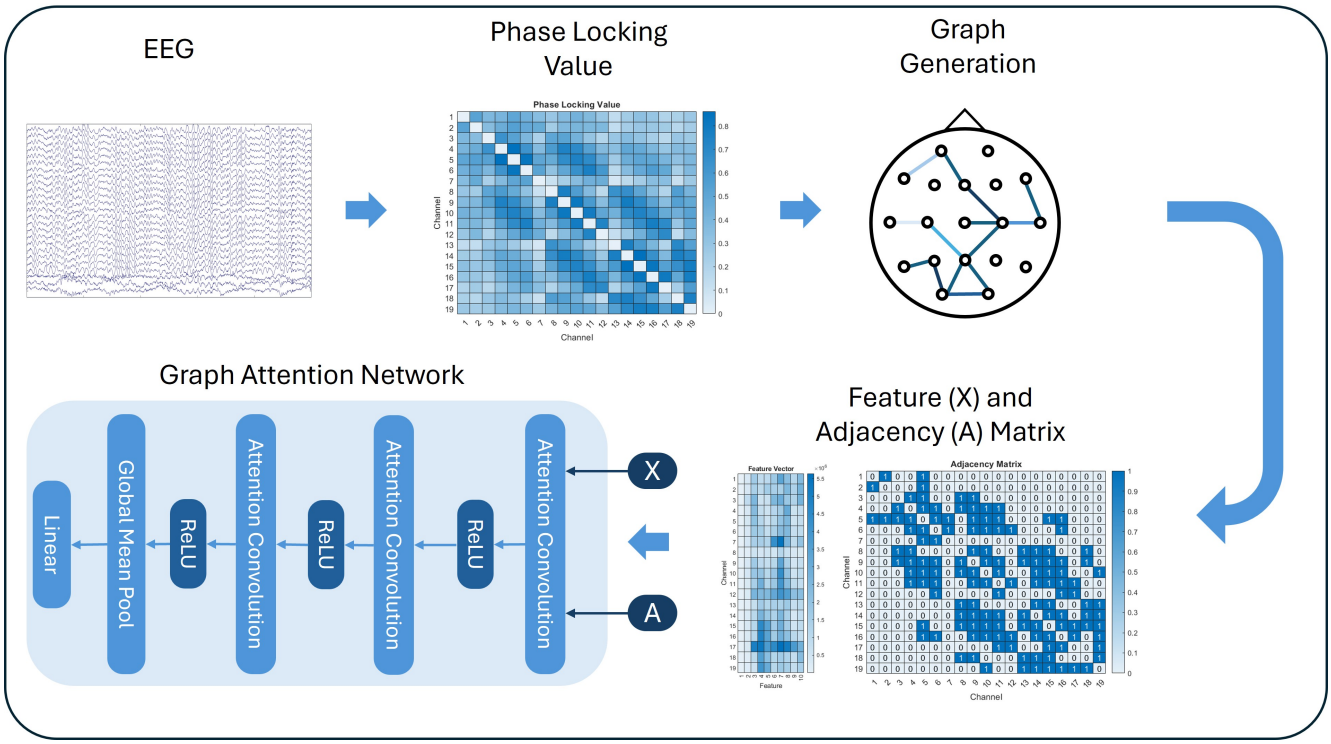

Figure 1. The proposed system architecture: using EEG to derive the unique phase coupling patterns between channels leading graph generation where Feature Matrix and Adjacency Matrix are derived to be classified by the network.

In this section, the methodology underpinning the proposed system architecture for the classification of EEG signals is shown, as illustrated in Figure 1. It harnesses EEG data to extract unique phase coupling patterns between channels, serving as the foundation for graph generation. Each channel's phase coupling information is analyzed to identify the relationships among various brain regions during motor imagery tasks. From these interactions, two essential components are derived: the feature matrix, which encapsulates relevant features such as band power and PLV that reflect the underlying neural activity, and the adjacency matrix, which represents the connections between channels based on their coupling strengths. These matrices are subsequently input into a simple GAT model. By modeling the EEG data as a graph, the proposed system aims to enhance classification accuracy through a deeper understanding of functional connectivity. This architecture embeds an innovative integration of traditional EEG analysis with advanced graph-based methodologies, potentially paving the way for improved performance in brain-computer interface applications.

2.1. Dataset

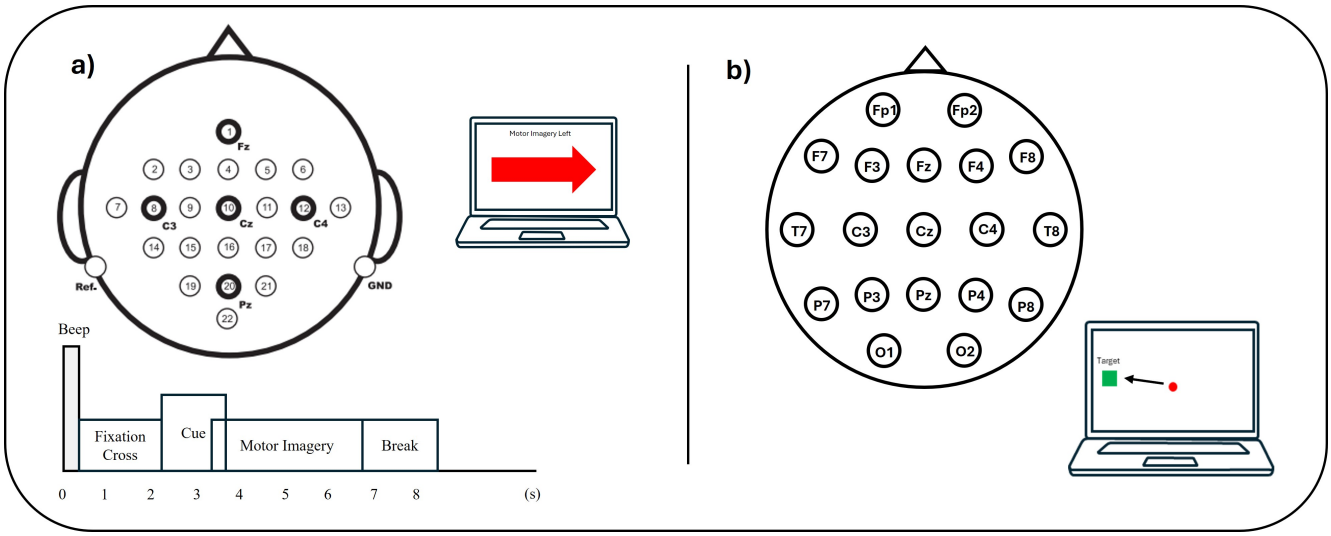

Figure 2. **(a)** Electrode configuration, timings and motor imagery example for dataset 1 (BCI Competition IV 2a. **(b)** Electrode configuration of the paradigm for dataset 2 (novel dataset with ALS patients).

Table 1. Summary of key parameters for EEG datasets.

Parameter	Dataset 1	Dataset 2
Participants	9	8
Classes	L and R Hand	L and R Hand
Total Trials	288 (144 per Class)	320 (160 per class)
Sessions	2 (different days)	4 (1-2 Months)
Sampling Rate	250Hz	256Hz
Electrodes	22	22
EOG Removal	Yes	Yes

2.1.1. Dataset 1: BCI competition IV 2a [15]

This dataset comprises EEG data from nine healthy participants undertaking a cue-based BCI paradigm. The paradigm included four motor imagery tasks: left hand (class 1), right hand (class 2), both feet (class 3), and tongue (class 4). In this work, only Class 1 and Class 2 are used to ensure a fair comparison against the second dataset which contains only left and right hand MI as described in Section 2.1.2. Each participant completed two sessions on different days, with each session consisting of six runs separated by short breaks. Each run included 48 trials (12 trials per class), totalling 288 trials per session. Prior to each session, a 5-minute EOG recording assessed eye movements, divided into three blocks: eyes open (2 minutes), eyes closed (1 minute), and eye movements (1 minute), they were recorded using a monopolar configuration with a sensitivity of 1 mV, solely for artifact processing and not for classification. Participants were seated comfortably in front of a computer screen throughout the sessions. Each trial began with a fixation cross and an acoustic warning tone. After 2 seconds, a cue (left, right, down, or up

arrow) appeared for 1.25 seconds, indicating the motor imagery task. Participants performed the task until the fixation cross disappeared at 6 seconds, followed by a short break. The experiment protocol can be seen in Figure 2a. Data was recorded using 22 Ag/AgCl electrodes with 3.5 cm inter-electrode distances, referenced to the left mastoid and grounded at the right mastoid. EEG signals were sampled at 250 Hz, bandpass filtered between 0.5 Hz and 100 Hz, and amplified with a sensitivity of 100 µV. A 50 Hz notch filter was used to suppress line noise.

2.1.2. Dataset 2: ALS [16]

This dataset includes EEG recordings from eight ALS patients aged 45.5 to 74, with revised ALS functional rating scale (ALSFRS-R) scores between 0 and 46 and time since symptom onset (TSSO) ranging from 12 to 113 months, with no disease progression reported during the study [16]. Patients, recruited from Penn State Hershey Medical Center ALS Clinic, had confirmed ALS diagnoses and no significant dementia. Data were collected with 19 electrodes placed according to the 10-20 system (FP1, FP2, F7, F3, FZ, F4, F8, T7, C3, CZ, C4, T8, P7, P3, PZ, P4, P8, O1, O2) referenced to linked earlobes and ground at FPz. Three EOG electrodes were used for artifact removal, with impedances kept below 10kΩ. Two g.USBamp system (g.tec GmbH) amplified signals, collected using BCI2000 software and MATLAB, following Penn State IRB protocol PRAMSO40647EP. Each patient completed four BCI sessions over 1-2 months, involving 4 runs per session, and 10 trials per class for each run (left hand, right hand, and rest), starting with a calibration run and followed by feedback runs where patients controlled the cursor movement via imagined grasping as shown in Figure 2b. This study focused on motor imagery (MI) data, totalling 160 trials over two months. The time frame of this data aligns with longitudinal BCI literature. By analyzing data longitudinally and employing new techniques, trends were captured in motor imagery decoding performance over time in ALS patients, to enhance understanding of BCI system adaptability.

2.2. Phase locking value

PLV is a method for calculating levels of phase coupling between EEG signals. This can provide information on the synchronicity of different nodes in a graph, in this case, channels of data. The Hilbert transform $H(s(t))$ is used to estimate the instantaneous phase $\phi(t)$ and amplitude $A(t)$ of a signal $s(t)$ as shown:

$$z(t) = s(t) + iH\{s(t)\} = A(t)e^{i\phi(t)} \tag{1}$$

where the instantaneous phase can be described by:

$$\phi(t) = \arctan\left(\frac{H\{s(t)\}}{s(t)}\right), \quad \phi \in [-\pi, \pi] \tag{2}$$

The phase difference between two channels can then be expressed by the subtraction of one from the other:

$$\phi_{m,n}(t) = \phi_i(t) - \phi_j(t) \tag{3}$$

Finally, the PLV of the trial can be calculated between m and n channels, where N is the number of samples in each trial and i is the imaginary unit:

$$\mathrm{PLV} = \left| \frac{1}{N} \sum_{t=1}^{N} e^{i\phi_{m,n}(t)} \right| \tag{4}$$

2.3. *Graph construction and distance measures*

Graphs are defined as $G(V,E)$, where V represents the nodes (points on a network) and E denotes the connections between the nodes V_i and V_j. Graphs can be constructed using various methods. In this study, PLV was employed to generate the graphs. Specifically, the strongest relationships are thresholded between each channel, excluding self-loops, to create a graph that represents the synchronicity between each pair of nodes. This representation can then be abstracted into an adjacency matrix A, which demonstrates the connections between nodes. Together with A, a feature matrix X is developed for each node at any given time. In this case, the inexpensive band power of the signal is used as a basis for experimentation.

Important measures in this method are the Graph Distance (GD) and Frobenius Norm (FN). These are used to assess the dissimilarity between graphs, providing information about the stability of the feature space. Considering that FN captures global differences and GD captures local node-to-node differences, the combination of the two can provide insights into clustering at different levels. Therefore, the two metrics offer greater confidence as clustering measures together than in isolation.

2.3.1. Frobenius Norm

$$\|A - B\|_F = \sqrt{\sum_{i=1}^{m} \sum_{j=1}^{n} |a_{ij} - b_{ij}|^2} \tag{5}$$

The Frobenius Norm provides a metric of comparison between two adjacency matrices by quantifying the difference between each corresponding element. Here, A and B are the matrices being compared, a_{ij} and b_{ij} are the elements at channel i, j, and m and n are the dimensions of the adjacency matrices, which are equal ($m = n$).

2.3.2. Graph Distance

The Graph Distance is the sum of the distances from each corresponding node in two graphs, G_1 and G_2. Typically, Graph Edit Distance is used, which seeks to determine how many node and edge changes are needed to transform one graph into another. This optimization can be complex and time-consuming, especially for weighted graphs. To mitigate this, the approach is approximated by calculating the sum of absolute differences between entries in two adjacency matrices. This provides an approximation of the distance between graphs based on their weighted adjacency matrices. The implementation is defined in Equation 6, where n represents the size of the adjacency matrix, which is $n \times n$, and a_{ij} and b_{ij} are the elements of the matrices:

$$\mathrm{GD}(A,B) = \sum_{i=1}^{n} \sum_{j=1}^{n} |a_{ij} - b_{ij}| \tag{6}$$

2.4. Graph attention network

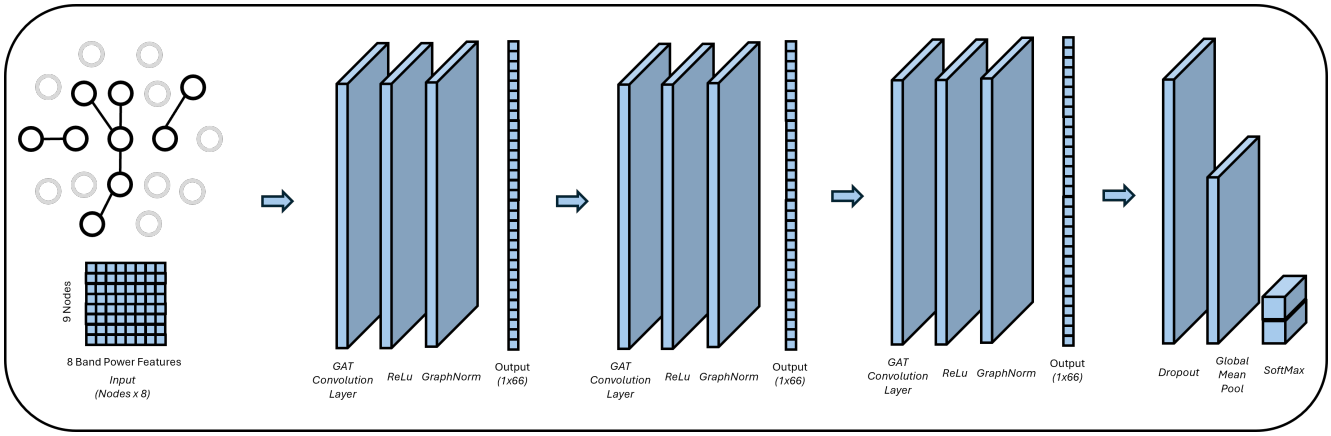

Figure 3. GAT model architecture.

In this study, the GAT is used to classify graph-structured data, as illustrated in Figures 1 and 3. Each graph $G(V,E)$ is represented by an adjacency matrix A and a node feature matrix X. The adjacency matrix is derived from a threshold on the PLV for each trial, with values above the threshold indicating connections. The feature matrix includes band power information from 8 to 40 Hz in 4 Hz increments as similar to the work by [17], taking inspiration from the famous filter-banks applied to Common Spatial Patterns (CSP) [18] resulting in a feature vector of size $n \times f$, where n is the number of channels and f is the number of features.

This approach combines spectral features (ERD/ERS) with the benefits of graph learning. This provides the GAT model with more granular frequency information, which could be overlooked in more traditional frequency boundaries for alpha (8–13Hz), beta (13–30Hz), theta (4–8Hz), and gamma bands (30Hz+). These bands are crucial for motor processing and play significant roles in motor imagery tasks across diverse patient and subject group, therefore they are important for the attention mechanism learning. This 4 Hz binned approach allows for a more detailed examination of power within each frequency sub-band, enabling the model to capture subtle variations in brain activity that may vary between tasks or subjects. Although this method increases computational complexity, the use of 4 Hz bins provides a balance between granularity and feasibility with our computational constraints in efforts to keep the model as small as possible. Allowing us to account for subject-specific fluctuations in frequency dynamics without increasing the computational load further.

The GAT model, implemented using PyTorch Geometric (2.5.0) [19] on a personal computer with an Intel Core i7 vPro CPU and 32GB RAM, employs three masked self-attention mechanisms to aggregate features from neighbouring nodes based on A [20]. It includes three GAT convolutional layers with ReLU activations and Graph Batch Normalization (see Figure 3). The model processes a feature matrix of $8 \times N$ (after thresholding, not all channels will be included as a valuable phase relationship) through layers with varying attention heads from 1 to 3, maintaining a computationally efficient setup with 22 hidden nodes per layer and an output size of $22 \times$ Heads. A dropout layer with $p = 0.5$ prevents overfitting.

Node features are averaged to produce a graph-level feature vector, which is passed through a sigmoid function to generate class probabilities. The Adam optimizer with cross-entropy loss was used. A 10-fold cross-validation approach was employed, shuffling the data to rigorously evaluate the generalizability

of the model. This method ensures that each fold of the dataset is used both for training and testing, providing a comprehensive assessment of the model's performance across different subsets of the data. Each model was trained for 250 epochs with a learning rate of 0.001 to optimize convergence and prevent overfitting. All testing data remained completely unseen by the model during training. This setup allows for a more accurate evaluation of the model's ability to generalize to new, unseen data.

3. Results

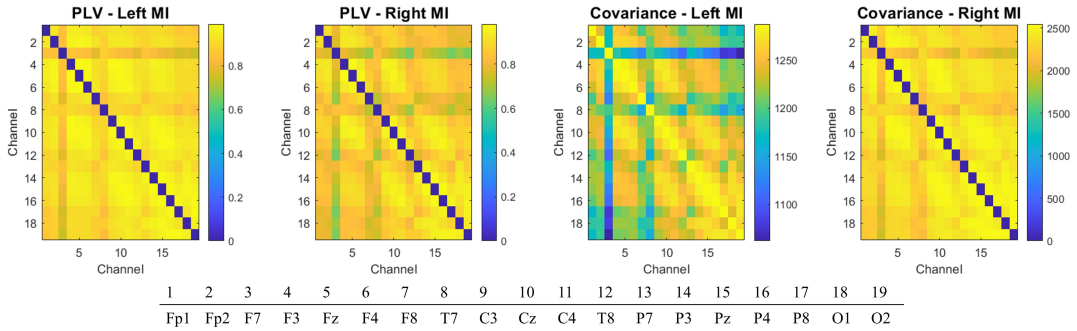

Figure 4. Average similarity measures over all trials for each class (left and right hand motor imagery with phase locking value and covariance) for Subject 1 in the ALS dataset.

Converting EEG data into a graph that accurately reflects neuronal connections is challenging, especially for graph classification. It is crucial to have a training set that captures task-specific features and provides a discriminative space for the classifier. As shown in Figure 4, covariance and PLV matrices for each class were computed with the further inclusion of Pearsons Correlation Coefficient (PCC). PCC and Covariance is simpler and less costly, while PLV offers more detailed information grounded in the neurophysiology. This was done using all available trials per subject. Feature engineering focused on identifying the class with the highest similarity and variability among EEG graphs using the FN and GD. Both metrics aim to find the lowest values, indicating stronger clustering within each class as mentioned previously.

Table 2. GD and Frobenius Norm across Dataset 1 and 2.

Dataset 1. Healthy participants

Adjacency Matrix	**Average GD**		**Average Frobenius Norm**	
	Left	**Right**	**Left**	**Right**
Covariance	64.25 ± 7.12	62.75 ± 7.57	3.56 ± 0.36	3.49 ± 0.41
PLV	33.34 ± 4.25	32.83 ± 3.54	1.94 ± 0.24	1.91 ± 0.21
PCC	28.18 ± 4.72	27.84 ± 4.69	1.77 ± 0.28	1.75 ± 0.29

Dataset 2. ALS patients

Adjacency Matrix	**Average GD**		**Average Frobenius Norm**	
	Left	**Right**	**Left**	**Right**
Covariance	46.02 ± 6.42	54.05 ± 15.36	2.51 ± 0.37	2.92 ± 0.69
PLV	29.09 ± 5.63	28.18 ± 5.60	1.96 ± 0.38	1.91 ± 0.38
PCC	46.48 ± 12.21	46.48 ± 7.69	2.74 ± 0.64	2.78 ± 0.49

Table 2 demonstrates why PLV should be selected as the primary measure of connectivity due to its stability performance across time and subjects, as evidenced by the GD and FN results, as well as the neurophysiological understanding we can leverage from PLV. Across ALS subjects, PLV consistently yielded lower and more stable GD and FN values compared to Covariance and PCC, comparing to Healthy where PLV achieved second best. PLV demonstrates less variation in the adjacency matrices, indicating that it better captures consistent brain connectivity patterns over time. For instance, in Dataset 2, PLV exhibited significantly lower GD values (29.09 ± 5.63, 28.18 ± 5.60) and FN values (1.96 ± 0.38, 1.91 ± 0.38) than Covariance and PCC, emphasizing its robustness. This stability is critical for longitudinal studies, particularly when analyzing datasets from neurodegenerative conditions such as ALS, where brain signal patterns may be more susceptible to noise and variability. Therefore, PLV's improved ability to capture neural interactions over time makes it an ideal metric for analyzing motor imagery data and other time-dependent EEG features in clinical and research contexts.

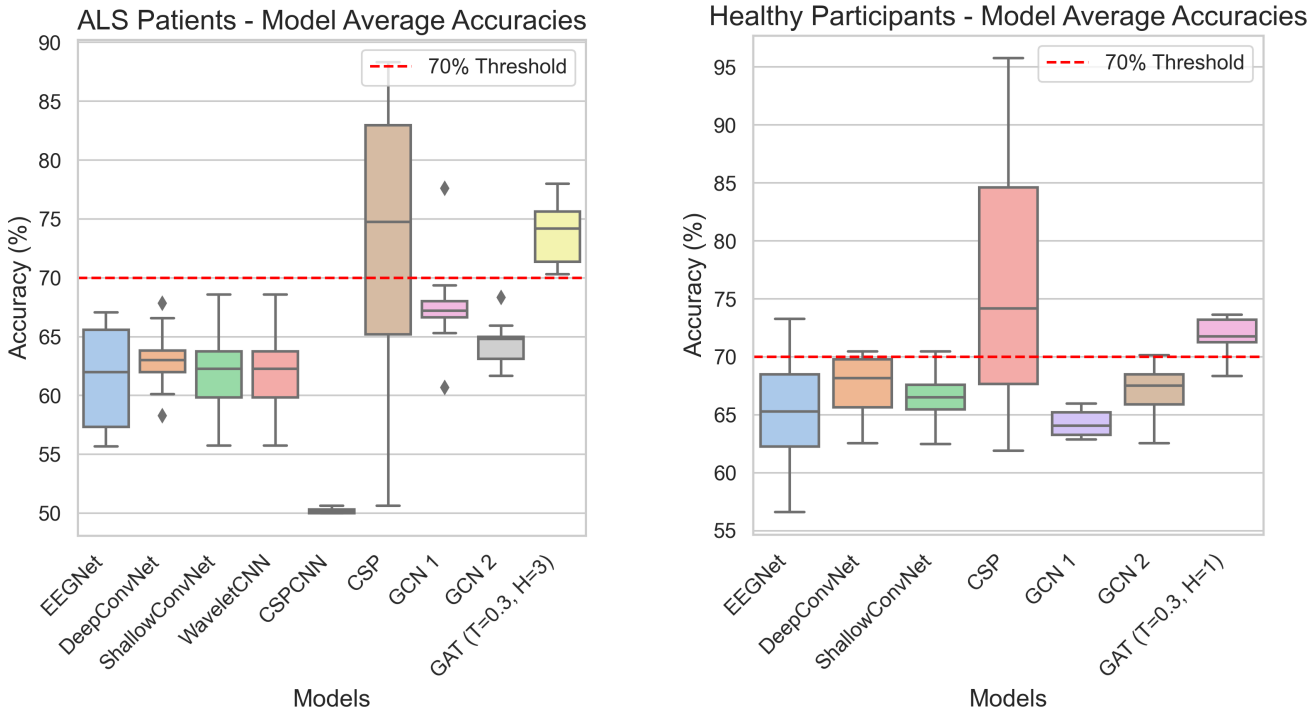

(a) Accuracies for ALS dataset using H=3

(b) Accuracies for Healthy dataset using H=1

Figure 5. Box plots of accuracies achieved with 10-fold cross validation on seven methodologies. PLV threshold = 0.3, Batch = 32, Learning Rate = 0.001 and Epoch = 250.

Figure 5 presents a comparative analysis of the proposed method against several state-of-the-art deep learning approaches across the two datasets, providing insight into each model's performance for every subject. The figure highlights the performance of seven models: CSP [21], EEGNet [22], DeepConvNet [23], ShallowConvNet [23], two custom GCN models, and the proposed method with GAT (H=3 for ALS patients and H=1 for healthy participants). EEGNet and both ConvNet variants were implemented using the official implementations by [22, 23], while CSP was executed with the MNE toolbox. Due to challenges in effectively reproducing the results of Wavelet-CNN [24] and CSP-CNN [17] on Dataset 1, the original findings are added as reported by the authors in Table 3. For effective comparison, our implementations of [24, 17] were applied based on the authors' documentation and

available code to the ALS dataset are shown in Figure 5 and Table 4. Detailed methodology and code are available in the GitHub repository** . The models were evaluated using 10-fold cross-validation (90% training, 10% testing), consistent with standard practices in the literature. Figure 5 demonstrates improved classification accuracies across the two datasets, exceeding the 70% threshold, with gains of 4.06% for ALS patients and 1.89% for healthy participants. The two GCN algorithms share a similar architecture with the proposed method, but the first lacks an attention mechanism and certain normalization layers and the second only the attention mechanism. These models were included to emphasize the critical role of the attention mechanism in enhancing classification accuracy. This comparative analysis not only highlights the strengths of the proposed approach, but also identifies areas for improvement relative to other state-of-the-art methods as will be discussed below.

Table 3. Comparison in accuracy of two-class classification on BCI competition IV 2a.

Subject	FBCSP*	CSP	CSSP	EEGNet	Deep ConvNet	Shallow ConvNet	Wavelet CNN*	CSP CNN*	GCN 1	GCN 2	GAT+PS
1	**91.33**	**77.71**	**71.8**	56.61	64.22	69.43	**76.67**	**90.26**	63.19	65.53	68.34
2	56.88	61.90	56.93	65.23	69.78	65.63	**72**	68.42	63.55	67.71	**71.51**
3	**93.05**	**91.71**	**93.37**	61.25	64.98	62.48	**90**	**95.46**	65.30	69.77	**71.18**
4	62.83	**70.76**	59.69	61.25	**70.42**	65.42	**73.33**	**78.47**	65.83	65.00	**71.67**
5	**88.2**	63.24	52.18	65.23	69.79	63.14	**83.33**	**91.32**	62.86	67.73	**73.65**
6	58.26	66.62	56.66	73.26	68.73	67.78	**80**	**72.59**	63.17	68.76	**73.33**
7	**92.01**	**70.86**	65.91	**71.48**	**70.47**	**70.46**	**82.67**	**94.8**	64.90	67.32	**73.61**
8	**95.85**	**95.76**	**96.16**	65.65	62.54	67.03	**80**	**97.22**	65.96	**70.14**	**72.88**
9	**92.03**	**86.90**	**93.41**	69.43	67.62	66.28	**80**	**94.1**	63.87	62.54	**70.87**
Average	81.16	76.16	71.79	65.49	67.62	66.41	79.78	86.96	64.29	67.17	71.89

***Reported model accuracies from original work**

Table 4. Comparison in accuracy of two-class classification on ALS dataset.

Subject	CSP	EEGNet	Deep ConvNet	Shallow ConvNet	Wavelet CNN	CSP CNN	GCN 1	GCN 2	GAT+PS
1	51.57	65.69	66.56	61.82	55.94	50.00	69.37	65.94	**70.31**
2	65.21	67.06	60.12	68.57	53.17	50.29	**77.59**	68.34	**77.05**
3	50.64	56.93	63.34	58.87	50.31	50.32	66.64	62.88	**71.36**
4	**88.31**	65.59	67.84	66.54	63.85	50.32	66.67	64.80	**74.19**
5	**82.97**	55.69	58.28	59.85	55.63	50.62	65.31	63.12	**75.62**
6	**75.40**	62.58	63.83	55.73	52.81	50.00	67.19	65.00	**75.31**
7	**74.76**	57.34	62.06	63.75	56.67	50.00	60.67	65.00	**70.67**
8	**83.16**	61.99	61.99	63.01	53.00	50.00	68.00	61.67	**78.00**
Average	71.50	61.61	63.00	62.27	55.17	50.19	67.68	64.59	74.06

Tables 3 and 4, demonstrate the individual subject splits per model ([18, 21, 25, 22, 23, 24, 26, 17]) with the accuracies above the 70% threshold highlighted. The results from the GAT+PS implementation reveal a compelling performance profile with both datasets. Despite its architectural simplicity, the proposed GAT model achieves results comparable to established methods such as CSP and common spatial subspace projection (CSSP). This suggests that with further refinement GATs can compete with, and in many instances surpass, more intricate models. This is especially relevant in scenarios where computational resources are limited, such as online applications. The limited depth and moderate number

**https://github.com/rishannp/Motor-Imagery---Graph-Attention-Network

of attention heads reduce the overall complexity, making the model less resource intensive to train and deploy. The use of GraphNorm [27] for stable training, global mean pooling, and dropout layers to simplify the final representation further optimizes performance without adding significant computational overhead or overfitting. These design choices make the model well-suited for applications requiring efficiency while still benefiting from the power of attention mechanisms.

4. Discussion

4.1. Enhanced ALS accuracies

The ALS dataset consisted of 8 patients with varying ALSFRS, TSSO, impairment, and age that are likely to affect individual performance. The results show that classification accuracy for ALS patients improves with GAT+PS compared to other deep learning models, which are more resource-intensive to train and deliver inferior results. All patients in Dataset 2 achieved accuracies above the threshold in a longitudinally gathered dataset, demonstrating the potential of GAT+PS. While these results are promising, they should be validated with matched controls and under consistent experimental conditions. The findings support Georgiadis's (2018) [10] hypothesis that certain neurological conditions may benefit when using PLV, leading to better BCI performance compared to models that do not incorporate spatio-phase representations. ALS patients achieved accuracies above 70%, despite primary observations of low sensorimotor rhythm in some patients (*e.g.*, Patient 2) [16] who typically perform lower. This suggests that BCIs using graph-based connectivity representations could be particularly effective for people with neurodegenerative diseases and patients with ALS with cognitive impairments. This approach, which integrates multiple frequency bands, spatial electrode representations, and redundant electrode identification with goals similar to those of [28], improves the specificity and generalization of the subject, as evidenced by the low standard deviations shown in Figure 5. The model achieved a notable accuracy of 74.06% on ALS data across four sessions of spaced data collection (10-Fold CV), showing potential for inter-session generalization compared to traditional methods. However, this warrants further investigation by performing cross-session evaluations in the future and online studies. By abstracting EEG signals into spatially coupled representations, GAT+PS captures more stable network connections over time, as indicated by the calculations in Table 2, making it a promising tool for real-world BCI applications, particularly for patients with variable EEG signals.

4.2. Inter-subject differences

Using pairwise f-tests to analyze variance, the results demonstrate significant improvements in inter-subject generalization compared to established models across both the healthy and ALS datasets. On the healthy dataset, GAT+PS exhibits significantly lower variance compared to FBCSP, CSP, CSSP, EEGNet, Wavelet CNN, and CSP-CNN (all $p < 0.001$), which emphasizes a statistically robust advantage. However, comparisons with Deep ConvNet, Shallow ConvNet, GCN 1, and GCN 2 show no significant difference in variance ($p > 0.05$).

On the ALS dataset, GAT+PS demonstrates a statistically significant variance reduction compared to CSP ($p < 0.001$), while showing no significant variance difference with EEGNet, Deep ConvNet, Shallow ConvNet, Wavelet CNN, CSP CNN, GCN 1, and GCN 2 (all $p > 0.05$). This outcome does not support

this model's potential for stabilizing cohort accuracies in ALS.

These results indicate that GAT+PS effectively reduces variance in the majority of cases for the Healthy dataset, while achieving a more limited reduction in the ALS dataset. These findings underscore the model's capability to mitigate inter-subject variability in several instances, even when lower mean accuracies are reported by other models. This observation is particularly notable in the ALS dataset, where variance differences are not statistically significant, yet overall performance is enhanced.

4.3. Cohort performance comparison

Performance comparisons between these two datasets are limited by differences in data collection methods, which affect the validity of patient-control comparisons. Nonetheless, the consistently high performance across both patient and healthy groups is a notable result that warrants further validation using additional publicly available datasets. All participants in the ALS dataset performed above the 70% threshold and only 1 out of 9 subjects falls below in BCI Comp IV 2a. Several factors contribute to the similar accuracies. First, PLV was selected for its stationarity independence [29], as it enhances the prospect of stable phase synchronization patterns capture in brain dynamics, making it a robust feature for classification. Additionally, similarities in electrode configurations may lead to more homogeneous EEG graph structures across datasets, allowing the model to effectively capture consistent trends which could be further verified by using datasets of varying electrode montages. The accuracies in Table 3 and 4 demonstrate that GAT+PS effectively captures subject-specific trends and achieves low variance; this attention mechanism may help buffer against spatio-temporal non-stationarity by emphasizing specific graphs during testing resulting in comparable performance across subjects. The analysis of attention scores, shown in Figure 6, reveals an interesting pattern: While the model consistently achieves high accuracies, the specific attention to node pairings during training rarely aligns with the learned patterns during testing. This suggests that although attention heads isolate subject-specific features during training, the model tunes effectively by focusing on different neural patterns across subjects during testing, contributing to its robust performance and potential ability to excel in a non-stationary environment.

However, when comparing GAT+PS to others (see Figure 5, Tables 3 and 4), it is evident that many studies rely on complex, heavily optimized architectures, potentially leading to overfitting. In contrast, the relatively simple GAT implementation still performs competitively, demonstrating significant potential for future improvement. Unlike models requiring extensive training epochs, this methodology establishes a strong baseline, illustrating that simpler models can still achieve substantial progress. Notably, WaveletCNN uses 5 cross-validation for dataset 1, compared to the 10-fold cross-validation in dataset 1. Another modification in the design approach is the implementation of CSP-CNN with a more streamlined filter bank design. Instead of generating over 30 filter banks as in the original method, only 8 filter banks spanning 8 to 40 Hz in 4 Hz increments are used. This relieves computational constraints and highlights potential scalability challenges in the original model. Although various forms of CSP offer high performance methodologies, as evidenced in Table 3, they can be enhanced through deep learning techniques, such as CSP-CNN, despite its computational inefficiency by needing over 30 filter banks. Incorporating spatial filtering may further optimise this GAT architecture by directing attention layers toward specific motifs, as observed in other works included in the comparisons. Other high performing deep learning models rely on complex architectures, which may be less practical for edge applications, an

area where GAT+PS has potential for innovation. This new approach shows promise outperforming or competing with the state of the art models.

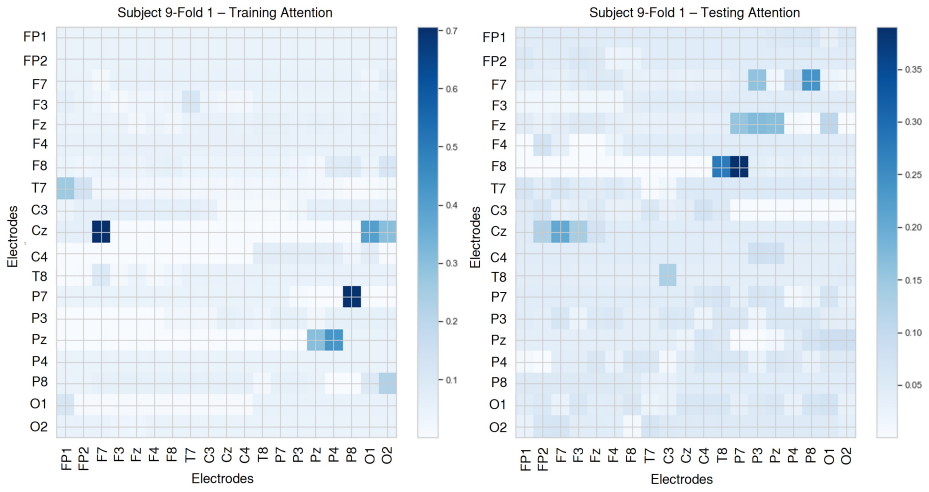

(a) Fold 1

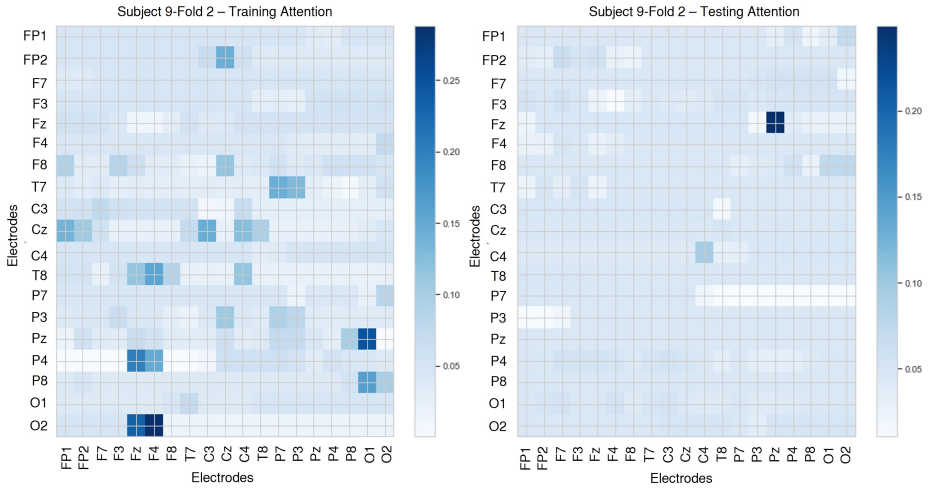

(b) Fold 2

Figure 6. Attention Scores from the final layer of the GAT Model on Patient 9 of the ALS Dataset. The figure shows how the attention heads value specific electrode pairs over Fold 1 and Fold 2 in the 10-fold Cross Validation task. Both Training Attention and Testing Attention are provided to understand how the model generalizes to unique patterns in the data.

Results suggest that increasing model complexity, such as the number of hidden features or attention heads, can sometimes lead to decreased accuracies. This trend is observed around the 22-feature mark, similar to the number of electrodes used. It appears that the GAT's performance benefits from a balanced representation of graph features across layers. The optimal number of attention heads is also dataset-specific and subject-specific. Investigation showed that, healthy participants performed best with H=1, and ALS patients with H=3. This insight may guide future research in optimizing the number of features and attention heads, ensuring they contribute effectively without introducing unnecessary complexity and reducing accuracies.

5. Conclusion

This study demonstrates that GATs offer a promising approach for BCI research, particularly in the context of subject-specific motor imagery decoding and neurodegenerative disease. While GAT implementation is efficient and competitive, further development and optimization are needed to fully realize its potential. Further development of advanced methodologies will enhance GAT efficacy and broaden its applicability across various BCI domains. The main contributions of this paper are as follows:

(1) A simplified graph attention network model is proposed, using phase-locking values for graph structure and band power as feature vectors. This model outperforms conventional methods like CSP and EEGNet, demonstrating high subject-specific performance with low variance, which could enhance BCI accessibility across diverse user groups.

(2) The PLV-GAT model achieves higher classification accuracy for both ALS patients and healthy users, suggesting it is particularly effective for individuals with traditionally challenging EEG patterns, such as those with ALS.

(3) The model maintains low variability across different subjects, even in extended, longitudinal datasets. By utilizing spatio-phase information, it addresses core challenges of EEG signal inconsistency, showing promise for robust, adaptive BCIs.

5.1. Future work

In exploring the potential of these models for motor imagery classification, several avenues for further development emerge. Current work demonstrates the feasibility of a model that leverages PLV as the graph structure and band power as the feature set for improved performance against state-of-the-art models. However, improvements are possible by incorporating a broader range of feature representations, such as cross-frequency coupling, which provides additional insights [11]. Improving the model could involve developing more sophisticated GAT architectures and introducing supplementary spatial filtering. Combining traditional methods like CSP with deep learning also appears promising and deserves further investigation within this framework. Expanding the complexity of these architectures, within practical limits, can enable us to match or surpass the performance of existing state-of-the-art models. Additionally, given evidence of subject generalization, investigating the minimum amount of training data required for stable inter-session decoding would further enhance the longitudinal feasibility of GAT and graph-based processing whilst testing this work in a causal manner. By addressing these areas, future research can build on the insights from this study, paving the way for more effective and efficient MI classification methods.

Supplementary data

The code to process this has been open-sourced and is available at: https://github.com/rishannp/Motor-Imagery---Graph-Attention-Network.

Acknowledgments

Funding: This work was supported by the EPSRC Doctoral Training Program (EPSRC Grant Reference: EP/W524335/1). The authors would like to acknowledge Dr Geronimo from Penn State University for

providing access to the data analyzed in this work.

Conflicts of interests

The authors declare there are no conflicts of interest.

Ethical statement

The study was performed in accordance with the Declaration of Helsinki and approved by the UCL Research Ethics Committee (23/07/2024, 26907/001).

Author's contribution

Rishan Patel: Conceptualization, Methodology, Software, Data Curation, Writing, Visualization. Ziyue Zhu: Visualization, Validation, Writing – Reviewing and Editing. Dai Jiang: Writing – Review Editing, Supervision.Barney Bryson: Supervision. Andreas Demosthenous: Supervision. Tom Carlson: Writing – Review Editing, Supervision

References

[1] Kübler A, Nijboer F, Mellinger J, Vaughan TM, Pawelzik H, *et al.* Patients with ALS can use sensorimotor rhythms to operate a brain-computer interface. *Neurology* 2005, 64:1775–1777.

[2] Perdikis S, del R Millan J. Brain-machine interfaces: A tale of two learners. *IEEE Syst. Man Cybern. Mag.* 2020, 6:12–19.

[3] Nihei K, McKee AC, Kowall NW. Patterns of neuronal degeneration in the motor cortex of amyotrophic lateral sclerosis patients. *Acta neuropathologica* 1993, 86:55–64.

[4] Zhang R, Li F, Zhang T, Yao D, Xu P. Subject inefficiency phenomenon of motor imagery brain-computer interface: Influence factors and potential solutions. *Brain Sci. Adv.* 2021, 6:224–241.

[5] Guger C, Edlinger G, Harkam W, Niedermayer I, Pfurtscheller G. How many people are able to operate an EEG-based brain-computer interface (BCI)? *IEEE Trans. Neural Syst. Rehabil. Eng.* 2003, 11:145–147.

[6] Blankertz B, Sannelli C, Halder S, Hammer EM, Kübler A, *et al.* Neurophysiological predictor of SMR-based BCI performance. *NeuroImage* 2010, 51:1303–1309.

[7] Zhang R, Xu P, Chen R, Li F, Guo L, *et al.* Predicting inter-session performance of SMR-based brain-computer interface using the spectral entropy of resting-state EEG. *Brain Topogr.* 2015, 28:680–690.

[8] Acqualagna L, Botrel L, Vidaurre C, Kübler A, Blankertz B. Large-scale assessment of a fully automatic co-adaptive motor imagery-based brain computer interface. *PLOS ONE* 2016, 11:e0148886.

[9] Daly I, Nasuto SJ, Warwick K. Brain computer interface control via functional connectivity dynamics. *Pattern Recognition* 2012, 45:2123–2136.

[10] Georgiadis K, Laskaris N, Nikolopoulos S, Kompatsiaris I. Exploiting the heightened phase synchrony in patients with neuromuscular disease for the establishment of efficient motor imagery BCIs. *J. NeuroEng. Rehabil.* 2018, 15:1–18.

[11] Klepl D, Wu M, He F. Graph neural network-based EEG classification: A survey. *IEEE Trans. Neural Syst. Rehabil. Eng.* 2024, 32:493–503.

[12] Almohammadi A, Wang YK. Revealing brain connectivity: Graph embeddings for EEG representation learning and comparative analysis of structural and functional connectivity. *Front. Neurosci.* 2023, 17:1288433.

[13] Sun H, Jin J, Daly I, Huang Y, Zhao X, *et al.* Feature learning framework based on EEG graph self-attention networks for motor imagery BCI systems. *J. Neurosci. Methods* 2023, 399.

[14] Demir A, Koike-Akino T, Wang Y, Erdogmus D. EEG-GAT: Graph attention networks for classification of electroencephalogram (EEG) signals. In *2022 44th Annual International Conference of the IEEE Engineering in Medicine & Biology Society (EMBC)*, Scotland, United Kingdom, July 11–15, 2022, pp. 30–35.

[15] Institute for Knowledge Discovery (Laboratory of Brain-Computer Interfaces). BCI competition IV 2a. https://www.bbci.de/competition/iv/, 2008. BCI Dataset. Graz University of Technology: Graz.

[16] Geronimo A, Simmons Z, Schiff SJ. Performance predictors of brain-computer interfaces in patients with amyotrophic lateral sclerosis. *Journal of neural engineering* 2016, 13.

[17] Bang JS, Lee MH, Fazli S, Guan C, Lee SW. Spatio-spectral feature representation for motor imagery classification using convolutional neural networks. *IEEE Trans. Neural Networks Learn. Syst.* 2022, 33:3038–3049.

[18] Ang KK, Chin ZY, Zhang H, Guan C. Filter bank common spatial pattern (FBCSP) in brain-computer interface. In *Proceedings of the international joint conference on neural networks*, Hong Kong, China, September 26, 2008, pp. 2390–2397.

[19] Fey M, Lenssen JE. Fast graph representation learning with PyTorch Geometric. In *ICLR Workshop on Representation Learning on Graphs and Manifolds*. 2019 .

[20] Veličković P, Casanova A, Liò P, Cucurull G, Romero A, *et al.* Graph attention networks. In *6th International Conference on Learning Representations, ICLR 2018*, Vancouver, Canada, April 30–May 3, 2018 .

[21] Ramoser H, Müller-Gerking J, Pfurtscheller G. Optimal spatial filtering of single trial EEG during imagined hand movement. *IEEE transactions on rehabilitation engineering : a publication of the IEEE Engineering in Medicine and Biology Society* 2000, 8:441–446.

[22] Lawhern VJ, Solon AJ, Waytowich NR, Gordon SM, Hung CP, *et al.* EEGNet: A compact convolutional neural network for EEG-based brain–computer interfaces. *J. Neural Eng.* 2018, 15:056013.

[23] Schirrmeister RT, Springenberg JT, Fiederer LDJ, Glasstetter M, Eggensperger K, *et al.* Deep learning with convolutional neural networks for EEG decoding and visualization. *Hum. Brain Mapp.* 2017, 38:5391–5420.

[24] Xu B, Zhang L, Song A, Wu C, Li W, *et al.* Wavelet transform time-frequency image and convolutional network-based motor imagery EEG classification. *IEEE Access* 2019, 7:6084–6093.

[25] Lemm S, Blankertz B, Curio G, Müller KR. Spatio-spectral filters for improving the classification of single trial EEG. *IEEE transactions on bio-medical engineering* 2005, 52:1541–1548.

[26] Jin J, Sun H, Daly I, Li S, Liu C, *et al.* A novel classification framework using the graph representations of electroencephalogram for motor imagery based brain-computer interface. *IEEE*

transactions on neural systems and rehabilitation engineering : a publication of the IEEE Engineering in Medicine and Biology Society 2022, 30:20–29.

[27] Cai T, Luo S, Xu K, He D, Liu TY, *et al.* GraphNorm: A principled approach to accelerating graph neural network training. *Proceedings of Machine Learning Research* 2020, 139:1204–1215.

[28] Aliakbaryhosseinabadi S, Dosen S, Savic AM, Blicher J, Farina D, *et al.* Participant-specific classifier tuning increases the performance of hand movement detection from EEG in patients with amyotrophic lateral sclerosis. *J. Neural Eng.* 2021, 18:056023.

[29] Sakkalis V. Review of advanced techniques for the estimation of brain connectivity measured with EEG/MEG. *Comput. Biol. Med.* 2011, 41:1110–1117.